Electronic Supplementary Material (ESI) for RSC Advances.

Supporting Information

Dual-Rotor Strategy for Organic Cocrystals with Enhanced Near-Infrared Photothermal Conversion

Xinyi Wen,[1#] Yixin Shao,[1#] Ye-Tao Chen,[1] Jiaxing He,[1] Shunli Chen,[1*] Li Dang,[1,2] Ming-De Li[1,2]

[1] College of Chemistry and Chemical Engineering, and Key Laboratory for Preparation and Application of Ordered Structural Materials of Guangdong Province, Shantou University, Shantou 515063, China

[2] Chemistry and Chemical Engineering Guangdong Laboratory, Shantou 515031, China.

*Corresponding author: chenxl@stu.edu.cn

Contents

Contents 1

1. The single-crystal data of cocrystals 2

1.1. The single-crystal data of cocrystals 3

1.2. Structure and morphology information of cocrystals shown by Mercury 4

2. UV-Vis-NIR absorption spectra of cocrystals 6

3. HOMO and LUMO molecular orbitals of cocrystals 6

4. HOMO and LUMO band diagram 6

5. Electron paramagnetic resonance spectra 7

6. Infrared vibrational spectra of cocrystals 7

7. Photothermal conversion experiments of cocrystals. 8

8. Thermal stability tests of cocrystals. 11

9. Femtosecond transient absorption spectra of cocrystals 12

10. The validity of dual-motor strategy. 14

1. The single-crystal data of cocrystals

F4TCNQ (2,3,5,6-tetrafluoro-7,7,8,8-tetracyanoquinodimethane, $C_{12}F_4N_4$, 98%) and MAT (9-methylanthracene, $C_{15}H_{12}$, 97%) were purchased from Bidepharm. DAT (9, 10-dimethylanthracene, $C_{16}H_{14}$, 98%) was gained from TCI. TCNQ (7,7,8,8-tetracyanoquinodimethane, $C_{12}H_4N_4$, 98%), acetonitrile (CH_3CN, AR) and methylene chloride (CH_2Cl_2, AR) were purchased from J&K. Unless otherwise specified, all of the chemical materials were used without further eradication.

All cocrystal samples were synthesized via solution volatilization method. In detail, MAT (11.5 mg) and TCNQ (12.2 mg) were together ultrasonically dissolved in the solvent of 9 ml acetonitrile. Similarly, DAT (12.3 mg) and TCNQ (12.2 mg) were dissolved in the solvent of 9 mL acetonitrile. DAT (12.3 mg) and F4TCNQ (16.5 mg) were dissolved in the solvent mixture of 3 ml acetonitrile and 3 ml dichloride. Then, these solutions were naturally volatilized by standing in the ambient condition with the temperature of 20±2 ℃ and the humidity of ~40%. Finally, three cocrystal materials, MAT-TCNQ (MTQ), DAT-TCNQ (DTQ) and DAT-F4TCNQ (DFQ), were obtained after about one week.

1.1. The single-crystal data of cocrystals

Table S1 Crystal data and structure refinement of cocrystal DFQ, DTQ and MTQ

	Complex MTQ	Complex DTQ	Complex DFQ
CCDC	2246243	2246244	2246245
Chemical formula	$C_{27}H_{16}N_4$	$C_{28}H_{18}N_4$	$C_{28}H_{14}N_4F_4$
Formula weight	396.44	410.46	482.43
Crystal system	monoclinic	triclinic	triclinic
Space group	$C_{2/m}$	$P\bar{1}$	$P\bar{1}$
a (Å)	11.1900(5)	6.7935(3)	7.7988(2)
b (Å)	13.4371(5)	8.9755(4)	8.4619(2)
c (Å)	7.0568(3)	17.3317(7)	16.7251(4)
α (deg)	90	102.064(4)	82.874(2)
β (deg)	98.472(3)	90.087(3)	80.374(2)
γ (deg)	90	96.951(4)	83.233(2)
V (Å^3)	1049.49(8)	1025.47(8)	1074.46(5)
Z	2	4	2
μ (mm^{-1})	0.596	0.628	0.970
Reflections collected	2115	8546	10185
Unique reflections	813	3769	3995
R_{int}	0.0153	0.0186	0.0204
GOF	1.093	1.040	1.069
R_1[a] [I > 2σ(I)]	0.0609	0.0389	0.0371
wR_2[b] [I > 2σ(I)]	0.1871	0.1103	0.0991
R_1[a] [all refl.]	0.0691	0.0407	0.0386
wR_2[b] [all refl.]	0.1970	0.1122	0.1007

[a] $R_1 = \sum(||F_o| - |F_c||)/\sum|F_o|$. [b] $wR_2 = [\sum w(F_o^2 - F_c^2)^2/\sum w(F_o^2)^2]^{1/2}$.

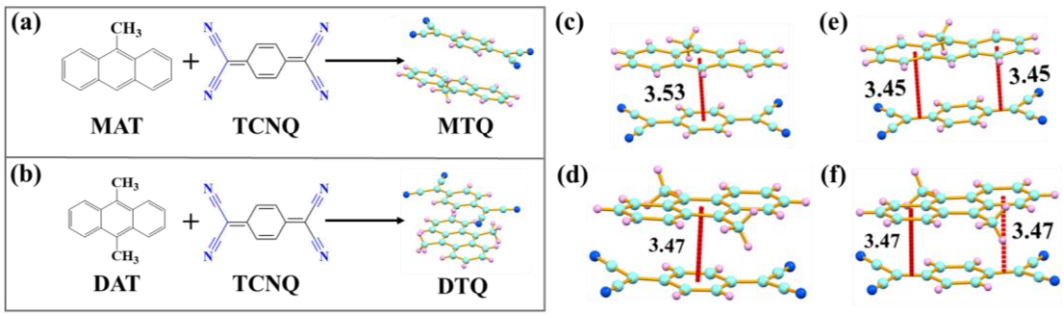

Figure S1. (a) Molecular structure and cocrystallization of MAT, TCNQ, and MTQ (a); MAT, TCNQ, and MTQ (b) cocrystal, along with corresponding powders. π–π interaction between donor and acceptor of MTQ (c) and DTQ (d). p–π interaction between donor and acceptor of MTQ (e) and DTQ (f). The crystal structures were resolved from the XRD curves obtained using an X-ray diffractometer (Bruker D8 ADVANCE).

1.2. Structure and morphology information of cocrystals shown by Mercury

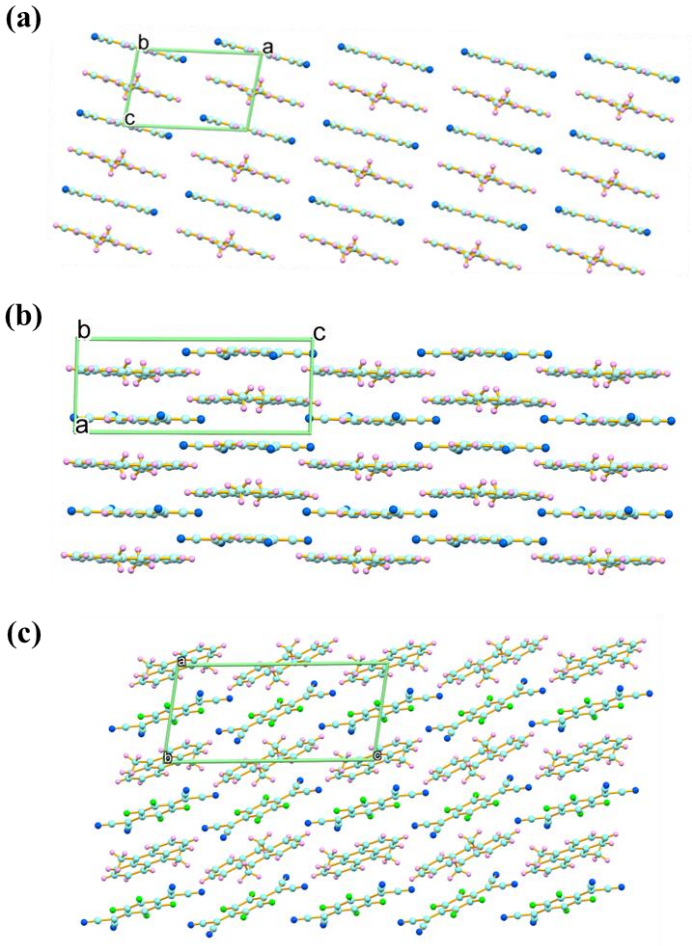

Figure S2. Cocrystal stacking structures of MTQ (a), DTQ (b) and DFQ (c).

It should be noted that, in subsequent analysis, the absorption spectra of samples were obtained by an UV-VIS-NIR absorption spectrophotometer (PerkinElmer Lambda 950). The infrared spectra were measured using the infrared spectrometer (Nicolet AVATAR360). The EPR spectra were obtained by an electron paramagnetic resonance spectrometer (Bruker E500-9.5/12). The thermogravimetric analysis was carried out by the differential scanning calorimeter (SHIMADZU DSC-60). The transient absorption spectra were acquired using a femtosecond transient absorption spectrometer (Ultrafast Helios Fire).

All theoretical calculations were carried out utilizing Gauss 16 software. The periodic structures for theoretical calculations were from the crystal structures resolved by the XRD technique. The basis group and functional used in the calculations are B3LYP/6-311G (d, p). Mercury software was used to measure the distances between donor and acceptor units; The energy level distribution was calculated using the density functional theory, and the hole-electron distribution was analyzed by Multiwfn 3.7 program.

The femtosecond transient absorption tests were performed based on the femtosecond Ti: Sapphire Regenerative Amplification Laser System (Coherent, Astrella-Tunable-F-1k) and fs-TA Spectrometer System (Ultrafast System, Helios Fire) systems. The amplifier is operated with a repetition rate of 1 kHz, a pulse width of 84 fs, and an output power of 7.14 W. By changing the time delay line to change the optical path difference between the pump light and the probe light, the three-dimensional spectrogram of the sample was obtained. Then the Surface Xplorer software was adopted to analyze and fit the transient spectrogram. The time resolution for transient absorption is about 120 fs.

2. UV-Vis-NIR absorption spectra of cocrystals

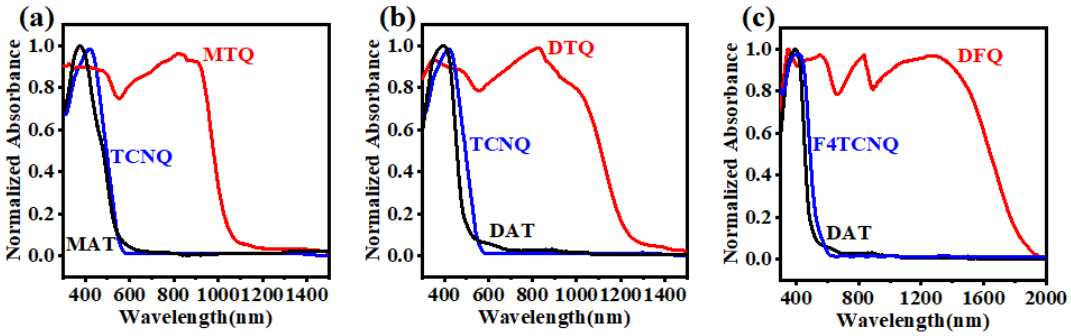

Figure S3. UV-Vis-NIR absorption spectrum of (a) MAT, TCNQ, and MTQ; (b) DAT, TCNQ, and DTQ; (c) DAT, F4TCNQ, and DFQ.

3. HOMO and LUMO molecular orbitals of cocrystals

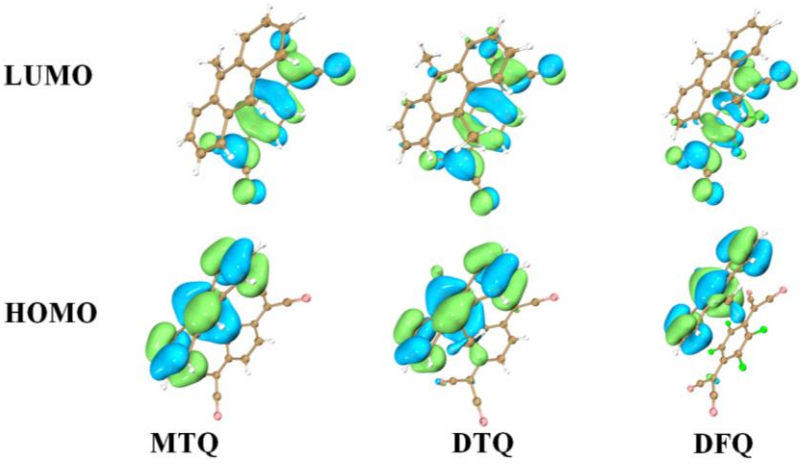

Figure S4. HOMO and LUMO molecular orbitals of MTQ, DTQ and DFQ.

4. HOMO and LUMO band diagram

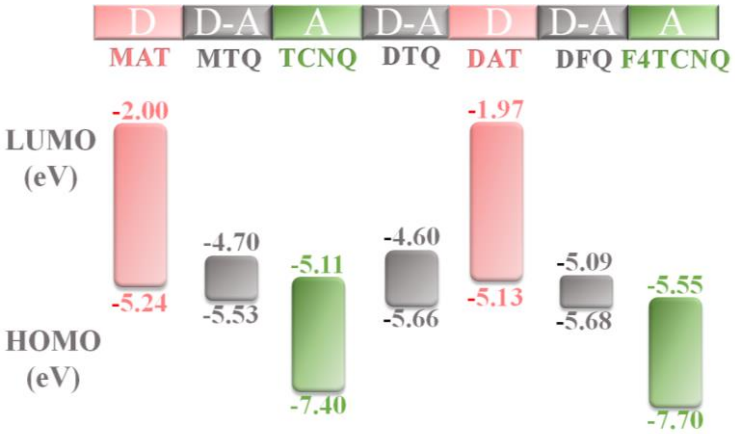

Figure S5. Band diagram of the donor (MAT, and DAT) and acceptor (TCNQ and F4TCNQ) and cocrystals (MTQ, DTQ and DFQ). (D: donor; A: acceptor).

5. Electron paramagnetic resonance spectra

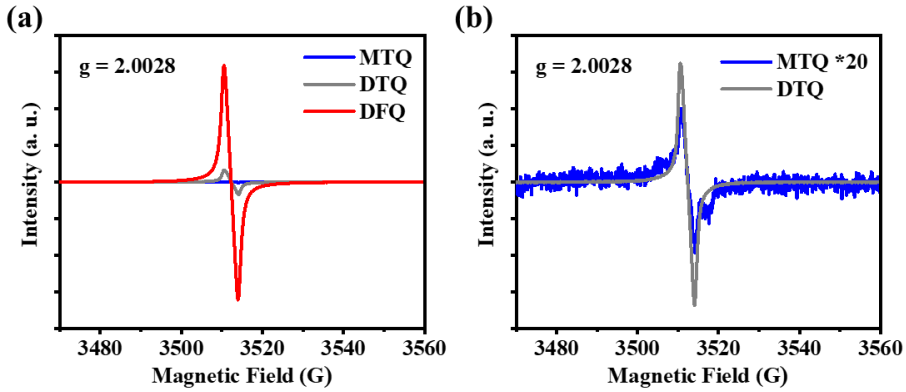

Figure S6. EPR spectra of MTQ/DTQ/DFQ (a) and the amplification of MTQ/DTQ (b).

The DCT values obtained from both the bond length parameters and the Fourier transform infrared absorptions show that there is a little difference in the DCTs of DTQ and MTQ cocrystals. However, their EPR spectra display an obvious intensity difference (Fig.1e). The observation seems reasonable because the EPR spectra is very sensitive to the resulting free radicals from the charge-transfer event in the cocrystals. Recently, we observed a weak but typical EPR signal with the g factor of 2.0025 for a similar cocrystal (TSB-F4TCNQ) with the DCT of ~0 (*Angew. Chem. Int. Edit.* 2024, in production, DOI: 10.1002/anie.202318628). Hence, the little difference in the DCTs of DTQ and MTQ cocrystals may produce an obvious difference in the concentration of free radicals and the EPR signal. Besides, their absorption spectra also have apparent difference with the absorption band of DTQ being ~150nm-broader than that of MTQ (Fig.1d).

6. Infrared vibrational spectra of cocrystals

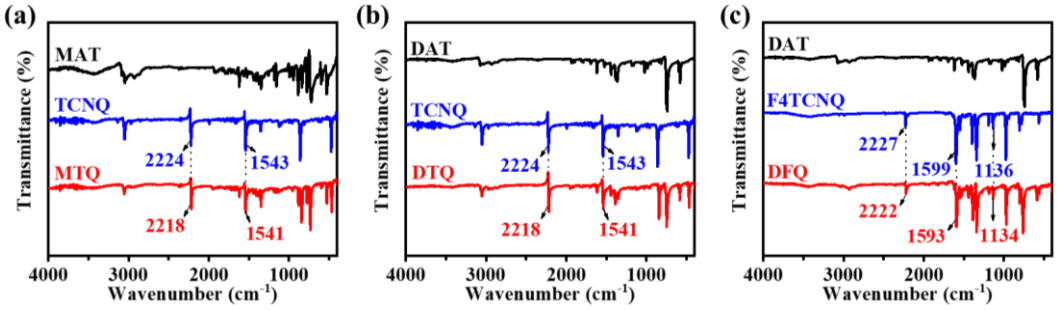

Figure S7. Infrared vibrational spectra of (a) MAT, TCNQ, and MTQ; (b) DAT, TCNQ, and DTQ; (c) DAT, F4TCNQ, and DFQ.

7. Photothermal conversion experiments of cocrystals.

The photothermal conversion efficiency of the co-crystal is determined according to the previous method.[3] Details are as follows:

Based on the total energy balance for this system:

$$\sum_i m_i C_{p,i} \frac{dT}{dt} = Q_S - Q_{loss}$$

$$\sum_i m_i C_{p,i} = m_{simple} \times C_{simple} + m_{\text{quartz}} \times C_{\text{quartz}}$$

Where m_{simple} and m_{quartz} are the mass of the sample and the quartz groove respectively. The m_{quartz} and C_{quartz} of the quartz-groove sample vessel are 1.26 g and 0.8 J•(g•°C)$^{-1}$, respectively. As for MTQ, m_{simple} and are 0.037 g and 1.15 J•(g•°C)$^{-1}$, respectively. And as for DTQ, m_{simple} and C_{simple} are 0.03 g and 1.01 J•(g•°C)$^{-1}$, respectively. And as for AT-P-TCNQ, m_{simple} and C_{simple} are 0.04 g and 1.04 J•(g•°C)$^{-1}$, respectively. And as for DFQ, m_{simple} and C_{simple} are 0.03 g and 0.87 J•(g•°C)$^{-1}$, respectively. Therefore, m_i and $C_{p,i}$ are the mass and specific heat capacity of the test system (crystal sample and quartz groove,), respectively. Q_S is the photothermal energy input when the near-infrared laser of 1064 nm irradiates the cocrystal sample, while Q_{loss} is the heat energy lost by the environment. When the temperature reaches its maximum, the system reaches equilibrium.

$$Q_S = Q_{loss} = hS\Delta T_{max}$$

Here h is the heat transfer coefficient, S is the surface area of the system, ΔT_{max} is one of the biggest temperature values. The efficiency of PT transformation is calculated like this:

$$\eta = \frac{hS\Delta T_{max}}{I(1 - 10^{-A_{808/1064}})}$$

where $I_{1064} = 1.0\ W$ is laser power and $A_{808/1064}$ is the absorbance of the samples at the wavelength of 1064 nm (MTQ=0.27, DTQ=0.74, DFQ =1.23) (Figure S13)

To obtain the hS, a dimensionless driving force temperature, θ is introduced as follows:

$$\theta = \frac{T - T_{surr}}{T_{max} - T_{surr}}$$

Where T is the temperature of MTQ, DTQ and DFQ, $T_{max/1064}$ (MTQ = 48.8 °C, DTQ = 78.2 °C, DFQ = 97.9 °C) is the maximum temperature of the system, and T_{surr} (19 °C)

is the initial temperature.

τ_s is the time constant of the test system:

$$\tau_s = \frac{\sum_i m_i C_{p,i}}{hS}$$

Then

$$\frac{d\theta}{dt} = \frac{1}{\tau_s}\frac{Q_s}{hS\Delta T_{max}} - \frac{\theta}{\tau_s}$$

When the laser is off, Q_s= 0, therefore $\frac{d\theta}{dt} = -\frac{\theta}{\tau_s}$, and $t = -\tau_s \ln\theta$

The time constant of the test system (τ_s) could be calculated from the slope of cooling time vs $\ln\theta$ for τ_s of MTQ, DTQ and DFQ are 144.18 s (Figure S10b), 124.51 s (Figure S11b) and 94.67 s (Figure S12b) respectively. And the photothermal conversion efficiency η_{1064} valuses of MTQ, DTQ and DFQ are 48.63%, 62.61%, and 73.57%.

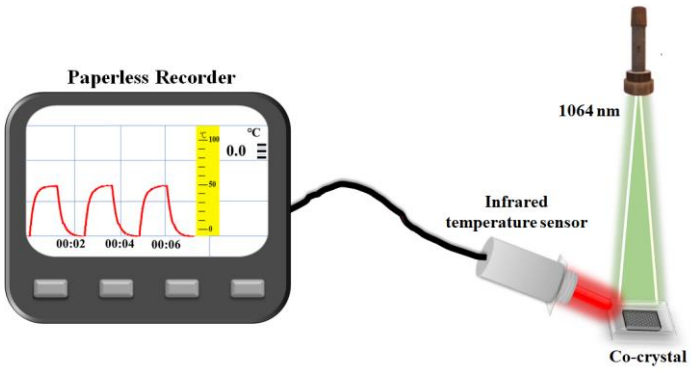

Figure S8. A device of near-infrared photothermal conversion is consisting of an 1064nm laser, a thermal sensor, paperless recorder and a quartz groove filled with test samples.

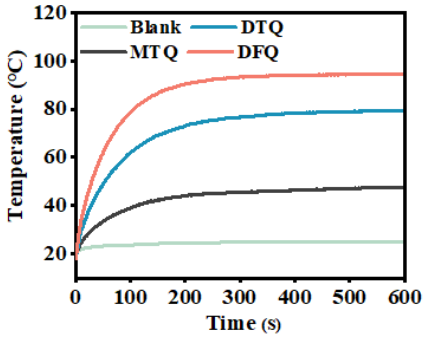

Figure S9. The heating curve of MTQ, DTQ, DFQ and blank control under 1064 nm laser.

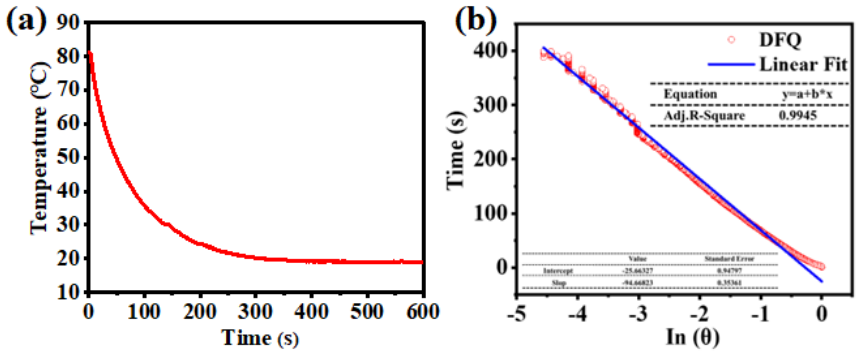

Figure S10. (a) The cooling curve of DFQ after the irradiation of 1064 nm laser (1.00 W/cm^2) and (b) its corresponding time-Inθ linear curve.

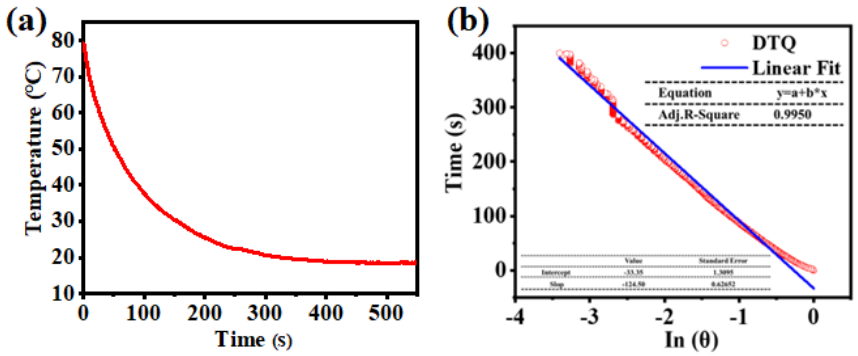

Figure S11. (a) The cooling curve of DTQ after the irradiation of 1064 nm laser (1.00 W/cm^2) and (b) its corresponding time-Inθ linear curve.

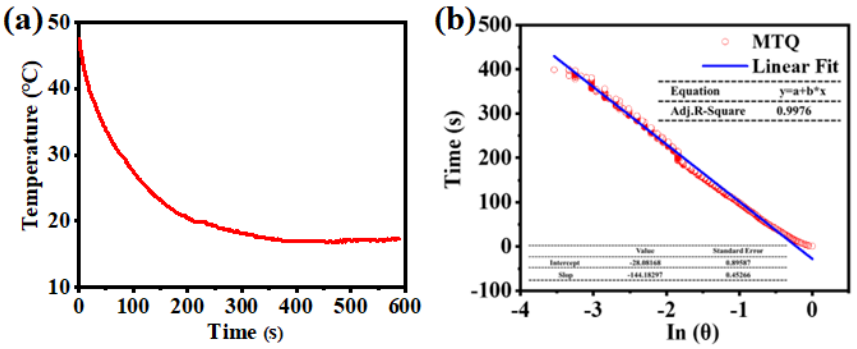

Figure S12. (a) The cooling curve of MTQ after the irradiation of 1064 nm laser (1.00 W/cm^2) and (b) its corresponding time-Inθ linear curve.

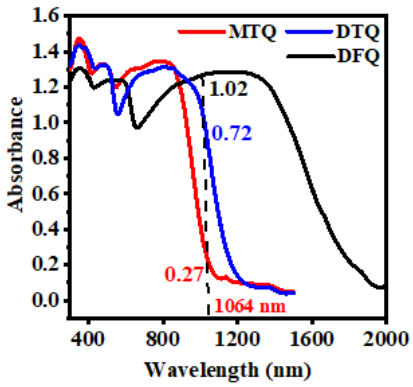

Figure S13. UV-Vis-NIR absorption spectra of MTQ, DTQ and DFQ.

8. Thermal stability tests of cocrystals.

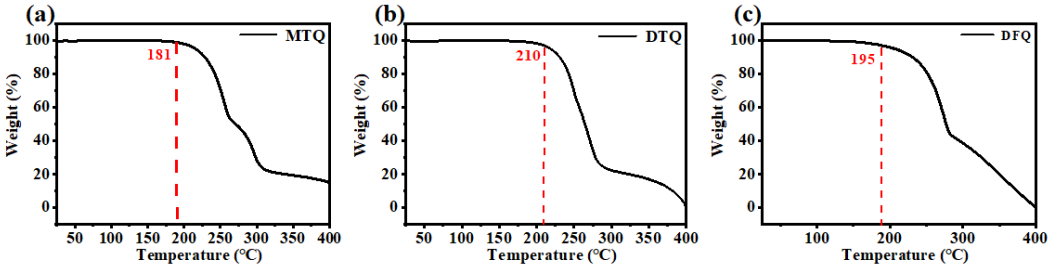

Figure S14. Thermogravimetric analyzer (TGA) of (a) MTQ, (b) DTQ, and (c) DFQ. (Testing condition: nitrogen environment and gas speed are 40 ml·min^{-1}; The heating rate is 10 °C/min.) The temperatures marked by the dashed red line indicate the decomposition points of cocrystals.

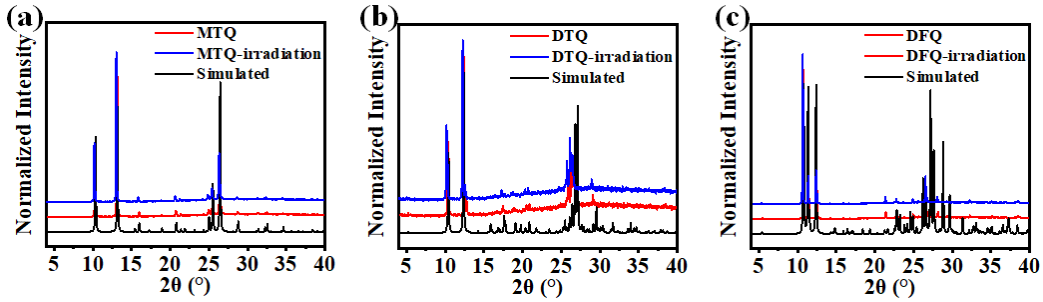

Figure S15. PXRD of (a) MTQ, (b) DTQ, and (c) DFQ and after 1064 nm irradiations (1.00 W/cm^2) for 1 h.

9. Femtosecond transient absorption spectra of cocrystals.

In Figures S16~S18, except the ESA band with positive signal, one or two peaks of ground-state bleaching (GSB) with negative signals were observed for all the DFQ/DTQ/MTQ cocrystals. The phenomena are similar to the results for the anthracene-TCNQ/F4TCNQ cocrystals reported in Ref.10.

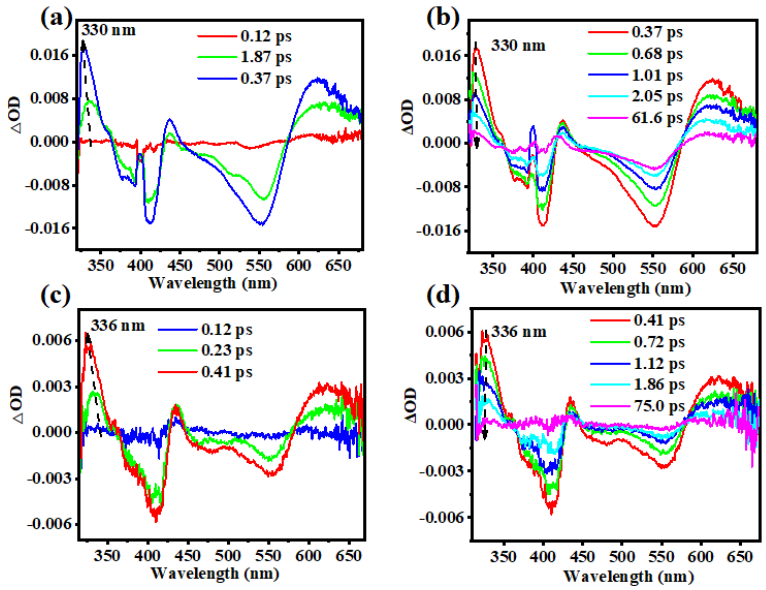

Figure S16. Transient absorption spectra of DFQ in different time ranges excited at 400nm (a and b) and 800 nm (c and d).

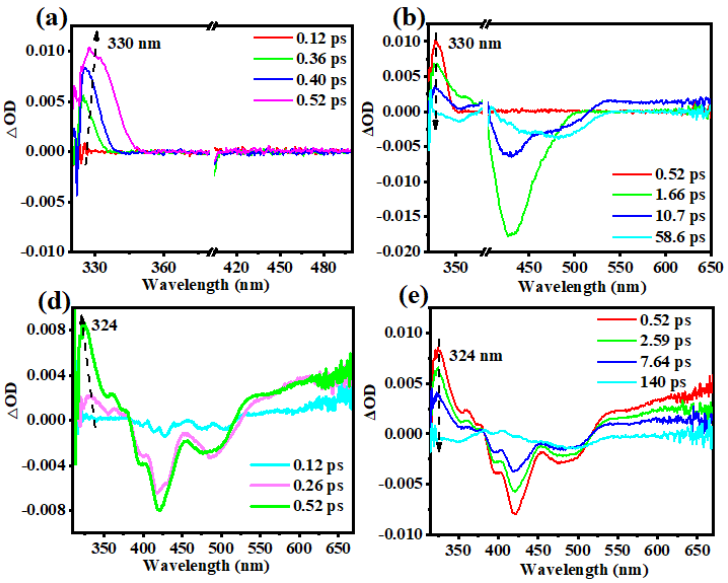

Figure S17. Transient absorption spectra of DTQ in different time ranges excited at 400nm (a and b) and 800 nm (c and d).

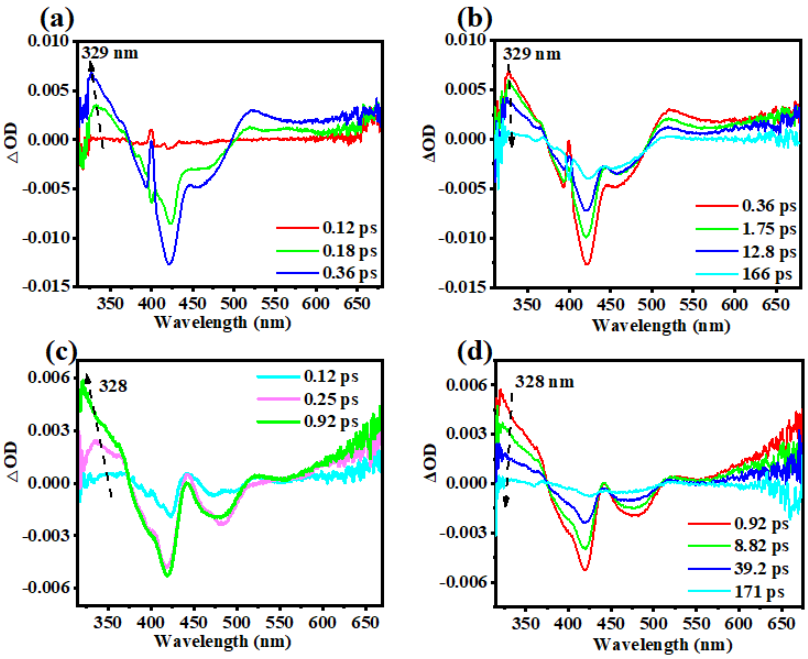

Figure S18. Transient absorption spectra of MTQ in different time ranges excited at 400nm (a and b) and 800 nm (c and d).

10. The validity of dual-motor strategy.

Table S2. The comparison of the decay lifetimes τ_1, τ_2 of ESA for DFQ/DTQ/MTQ in this work and anthracene-TCNQ/F4TCNQ reported previously. The fitting equation of the decays was shown in the caption of Figure 3. $\boldsymbol{A_{inf}}$ indicates the contribution of a decay process with very long lifetime.

D-A cocrystals	Fitting parameters (Excitation@800 nm)						DCT	η	Literature
	τ_1 (ps)	A_1	τ_2 (ps)	A_2	Inf	A_{inf}			
DFQ	0.79	89.0%	12.4	10.6%	—	0.4%	0.226	73.6%	This work
DTQ	3.4	45.2%	20.4	53.1%	—	1.7%	0.087	62.6%	
MTQ	5.4	26.0%	50.5	72.4%	—	1.6%	0.084	48.6%	
anthracene-F4TCNQ	2.7	64.6%	15.2	33.8%	—	1.6%	0.214	57.0%	Ref. 10 *ACS Appl. Mater. Interfaces* **2022**, 14, 28781−28791
anthracene-TCNQ	2.3	32.1%	77.9	60.3%	—	7.6%	0.096	60.5%	

To better illustrate the validity of dual-motor strategy to improve the PTC ability of cocrystals, we made a more careful comparison of MTQ (methylanthracene-TCNQ) and DTQ (dimethylanthracene-TCNQ) with the anthracene-TCNQ cocrystal reported in Ref.10. To make a straight comparison, the PTC efficiency $\boldsymbol{\eta}$, the decay lifetimes of ESA from fs-TA and the DCT values for the MTQ/DTQ/DFQ and anthracene-TCNQ/F4TCNQ cocrystals are shown in Table S2.

Dual-motor mechanism was supported by the comparison of DFQ and anthracene-F4TCNQ cocrystals with close DCT values:

Compared to the PTC efficiency η (57.0%) for the anthracene-F4TCNQ, the obvious higher η (73.6%) for the DFQ supports the validity of dual-motor mechanism. More importantly, the common rule works well that the faster nonradiative charge recombination largely corresponds to the higher PTC efficiency, and the ultrafast decay of ESA often dominates the PTC property of cocrystals (*J. Phys. Chem. Lett.* **2024**, 15, 68–75). As is clearly shown in Table S2, both the two decays of ESA with the lifetimes of τ_1 and τ_2 for the DFQ are faster than those for anthracene-F4TCNQ cocrystal. Especially, the first ultrafast decay with the lifetime of τ_1 (0.79 ps) and the weight factor of A_1 (89.0%) of DFQ is less than a third of that (2.7 ps) for anthracene-F4TCNQ

cocrystal.

The conflict with the rotor mechanism comes from the comparisons of DTQ, MTQ and anthracene-TCNQ cocrystals with close DCT values:

However, the η (62.6%) for the DTQ is only a little higher than that (60.5%) for the anthracene-TCNQ. Furthermore, the η (48.6%) for the MTQ is significantly smaller than that for the anthracene-TCNQ. This observation seems to conflict with the rotor mechanism.

To understand the possible internal reasons, we first compare their decay processes of ESA. The first ultrafast decays with the lifetime of τ_1 (3.4 ps/5.4 ps) and the weight factor of A_1 (45.2%/26.0%) for the DTQ/MTQ are slower than that (2.3 ps) with the weight factor of A_1 (32.1%) for the anthracene-TCNQ; but the second decay with the lifetime of τ_2 (20.4 ps/50.5 ps) and the weight factor of A_2 (53.1%/72.4%) for the DTQ/MTQ are faster than that (77.9 ps) with the weight factor of A_2 (60.3%) for the anthracene-TCNQ. So, these two decays seem to have a nonlinear additive contribution to the final PTC efficiency η while the first ultrafast decay of ESA with a certain weight factor still dominates the PTC property of cocrystals. The possible nonlinear additive phenomenon is also observed for other cocrystals (*J. Phys. Chem. Lett.* **2024**, 15, 68–75).

From the perspective of D/A molecular structure, the rotor mechanism may rely on the structural match and stacking distance of D/A units, which affect the possible free space for rotor rotation. After a careful comparison of the stacking structures of DFQ/DTQ/MTQ (Figures 1c, S1e,f) and anthracene-TCNQ/F4TCNQ (Figure 1k,l in Ref.10), we found that adding two methyl groups to anthracene induced a certain translation of stacking plane of DAT and F4TCNQ in the DFQ. This is the reason responsible for that there is only one p–π interaction in the DFQ, while two p–π interactions exist in the DTQ/MTQ and anthracene-TCNQ/F4TCNQ. Fortunately, this translation of stacking plane provides the possible free space for the methyl-rotor rotation in the DFQ.

The long-lived decay with a very small weight factor of A_{inf}~ 0.4%/1.7%/1.6% for the DFQ/DTQ/MTQ cocrystals:

It is really that many of the kinetic traces in Figure 3a,b do not decay to zero with much longer lifetime compared to the τ_1/τ_2. As is clearly shown in Table S2, the long-lived decay displays a very small weight factor of A_{inf}~0.4%/1.7%/1.6% for the

DFQ/DTQ/MTQ cocrystals, and its influence is neglected in this work. Actually, this long-lived decay may come from the possible intersystem crossing and subsequent decay process as observed in other F4TCNQ-based cocrystals (*J. Phys. Chem. Lett.* **2024**, 15, 68–75; *ChemSusChem* **2023**, 16 (14), e202300644).